Advanced Composite Materials
Publication details, including instructions for authors and subscription information:
http://www.tandfonline.com/loi/tacm20

Novel Test Method for Mixed Mode II and III Interlaminar Fracture Toughness

Hiroshi Suemasu [a], Atsushi Kondo [b], Katsuhisa Gozu [c] & Yuichiro Aoki [d]

[a] Department of Engineering and Applied Sciences, Sophia University, 7-1 Kioicho Chiyodaku Tokyo, Japan
[b] Department of Engineering and Applied Sciences, Sophia University, 7-1 Kioicho Chiyodaku Tokyo, Japan
[c] Department of Engineering and Applied Sciences, Sophia University, 7-1 Kioicho Chiyodaku Tokyo, Japan
[d] Japan Aerospace Exploration Agency, 6-13-1 Osawa Mitakashi Tokyo, Japan

Version of record first published: 02 Apr 2012.

To cite this article: Hiroshi Suemasu , Atsushi Kondo , Katsuhisa Gozu & Yuichiro Aoki (2010): Novel Test Method for Mixed Mode II and III Interlaminar Fracture Toughness, Advanced Composite Materials, 19:4, 349-361

To link to this article: http://dx.doi.org/10.1163/092430410X504143

VSP

Advanced Composite Materials 19 (2010) 349–361

ADVANCED COMPOSITE MATERIALS
brill.nl/acm

Novel Test Method for Mixed Mode II and III Interlaminar Fracture Toughness

Hiroshi Suemasu [a,*], **Atsushi Kondo** [a], **Katsuhisa Gozu** [a] **and Yuichiro Aoki** [b]

[a] Department of Engineering and Applied Sciences, Sophia University, 7-1 Kioicho Chiyodaku Tokyo, Japan

[b] Japan Aerospace Exploration Agency, 6-13-1 Osawa Mitakashi Tokyo, Japan

Received 3 July 2009; accepted 5 October 2009

Abstract

A novel test method is proposed to evaluate mixed mode II and III interlaminar fracture toughness of composite laminates. The method is a well-improved test method of the split cantilever test method and easy to conduct, while a computational analysis is necessary to specify the critical toughness values. The aim of the test is to obtain mixed mode fracture toughness. The twisting force that exists in the case of the split cantilever test method is avoided by making the specimen symmetric by introducing two symmetrically located delaminations. By the present method, the two cracks grow stably keeping their configuration with the increase of applied displacement, that is, stable self-similar crack growth is realized. The energy release rate can be numerically evaluated from the experimentally obtained data, such as, the applied load (or applied displacement) as well as the crack configuration. The energy release rate varies along the curved crack front and the dependence of the mixed mode critical energy release rate on the ratio of the mode components can be obtained by one test trial. The method can be conveniently used to roughly estimate the failure criterion for mode II and III mixed mode Interlaminar fracture.

Keywords

Mixed mode fracture toughness, interface crack, experiment, finite element analysis

1. Introduction

Laminated composites are used particularly for aerospace structures because of their high specific strength and stiffness. However, the laminated composite structures subjected to static, impact and/or cyclic loads may have significant interlaminar damage as a result of their insufficient interlaminar toughness. So, the interlaminar fracture toughness is regarded as an important index of the failure tolerance of the laminates. Considering that not only interlaminar normal (mode I) but

* To whom correspondence should be addressed. E-mail: suemasu@sophia.ac.jp
Edited by JSCM

 DOI:10.1163/092430410X504143

also in-plane shear (mode II) and out-of-plane shear (mode III) stress field causes delamination propagation, the values of all three individual and/or mixed interlaminar toughnesses must be evaluated to fully characterize the interlaminar fracture property of the composite laminates by using appropriate test methods.

There have been numerous studies concerning a test method to measure interlaminar fracture toughness because of its importance. The mode I fracture toughness of the laminated composites is well measured by DCB (double cantilever beam) test method [1–5]. The mode II fracture toughness of the laminated composite is also obtained through comparatively simple ENF (end-notched flexure) test method [1, 5, 6]. Mixed normal and in-plane shear (mode I and II) fracture test can also be conducted through MMB (mixed mode bending) and CLS (cracked lap shear) test method [1, 2]. There are experimental techniques for measuring mode III proposed by several workers [7–11], such as rail shear test and ECT (edge cracked torsion) test method, which are not so easy to perform as those proposed for measuring mode I and II fracture toughnesses.

Szekrenyes [12] has proposed a PENF test method, which is a combination of the ENF test and MSCB method to measure a mixed mode II and III fracture toughness using a beam-like specimen. De Morais and Pereira [13] have proposed an elaborate test method where the mixed mode condition is realized by two orthogonal moments parallel and transverse to an edge delamination of rectangular laminate. The test methods realized failure due to mixed mode II and III condition. However, accurate assignment of the mixed mode failure may not be possible owing to the non-uniform stress condition at the crack front created by those test methods. There needs to be some support using numerical analysis to get accurate mixed mode fracture toughness. Test methods to measure mixed mode I and III fracture toughness and that of all three components have not been proposed yet to our knowledge.

Though a split cantilever bending test method was proposed as a test method to evaluate pure mode III fracture toughness [14], the later work revealed that the energy release rate distribution along the crack front consisted of not only a mode III component but also a significant mode II component. In the present study, we will propose a modified SCB test method that is easy to conduct and from which it is possible to evaluate a wide range of mixed mode II and III fracture toughnesses by a single test by using a finite element method.

2. Double-Notched Split Cantilever Beam Test

2.1. Theoretical Assessment

The specimen configuration is shown in Fig. 1. Two cracks are introduced and the inside part of the cracked portion of the specimen is twice as thick as the outside portions so that not only is the specimen symmetric about the center surface, but also half of the specimen is also symmetric about the surface of the crack. The center cracked portion of the specimen is vertically loaded parallel to the crack face and both side portions are simply-supported. The specimen bends without twisting

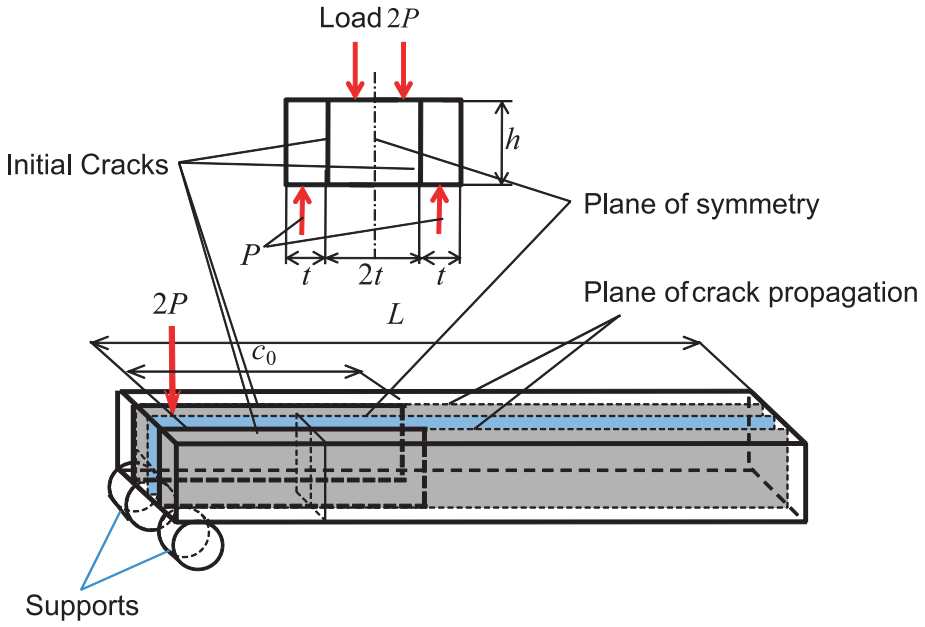

Figure 1. Specimen configuration of the double-notched split cantilever beam test method. This figure is published in color on http://www.ingentaconnect.com/content/vsp/acm

owing to its symmetry, and bending and shear stresses occur in the cross-sections of the cracked portions of the specimen, as shown in Fig. 2. Both bending and shear stresses are opposite at the inside and outside cross-sections.

At the beginning (when the crack front is straight), the bending stress contributes to the mode II component of the energy release rate, while the shear stress contributes to the mode III component. A critical condition of crack propagation is initially achieved at the edge portions of the crack front owing to the high bending stress. The cracked area spreads from both edges to the center portion of the beam and the crack front changes its shape from the initial straight one to a curved one. Finally, the two center portions of the cracks start growing and both cracks grow steadily while keeping a similar curved shape $c(y)$ with the increase of the applied displacement, as shown in Fig. 2. The curved crack shape is kept almost unchanged during the fracture test hereafter, as described in the next section. The distributions of the stresses are different from the initial state due to the curved crack front. The stresses are still opposite at the inside and outside cross-sections as shown in Fig. 2(b). As no opening force exists, the mode I component does not exist and both mode II and III components appear as a function of the curved shape of the crack front, as inferred from Fig. 2(c). As the cracks grow stably with the increase of the applied displacement, whose crack fronts just satisfy the critical condition, the mixed mode II and III fracture toughnesses can be obtained by analyzing the energy release rate along the curved crack front with an appropriate technique, such as the finite element method.

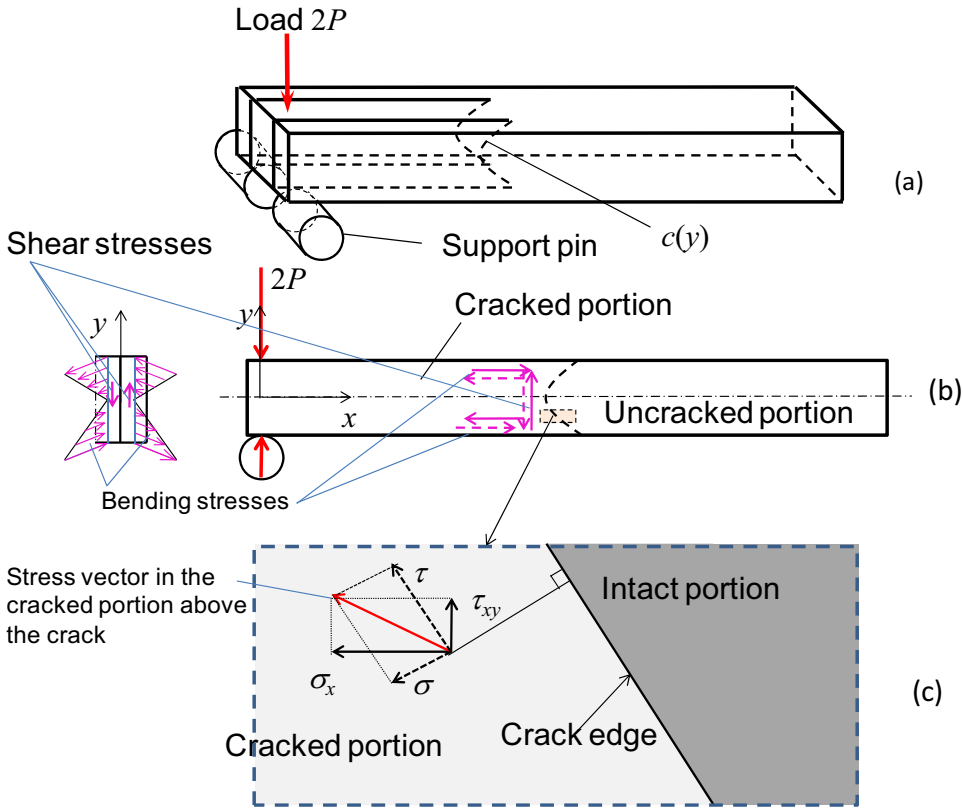

Figure 2. Concept of the double-notched split cantilever beam test method with curved crack front: (a) configuration of the specimen; (b) bending stress and shear stress in the cracked portion; (c) stress distribution in the outer portion near the crack front. This figure is published in color on http://www.ingentaconnect.com/content/vsp/acm

The crack propagation is basically stable, like the DCB test method when the displacement control test is conducted. The proof can be done by a method similar to that used for the DCB test.

2.2. *Test Fixture and Specimen Preparation*

A test fixture made for the present study is shown in Fig. 3. Two horizontal round pins support the bottom surface of the outer-portions of the specimen. The pins being sufficiently stiff can slide in the block to adjust specimen thickness. A vertical bar with round head applies downward displacement to the center portion of the specimen. A ball bearing supports the vertical bar to prevent it from tilting.

Specimens were prepared by gluing three acrylic plates using an epoxy adhesive agent so as to easily observe the shape of the crack front with the naked eye. One plate is twice as thick as the rest. PTFE films (20 μm thick) were placed at both end portions of the plates to make the adhesive as uniform as possible. The one end was

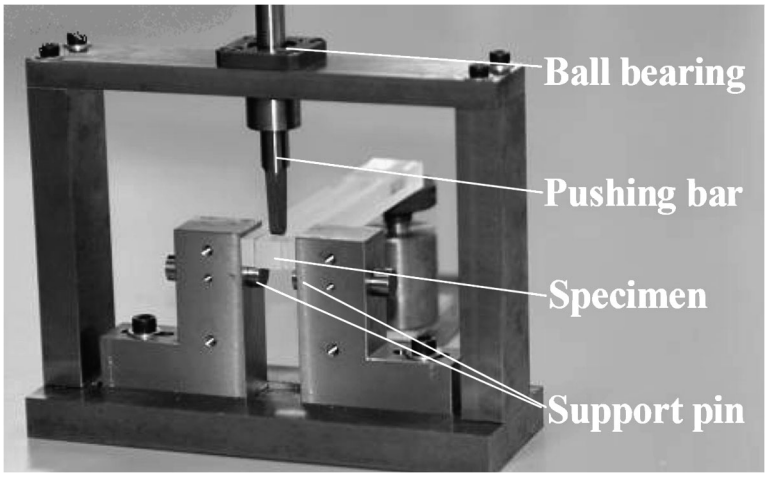

Figure 3. Fixture for the double-notched split cantilever test.

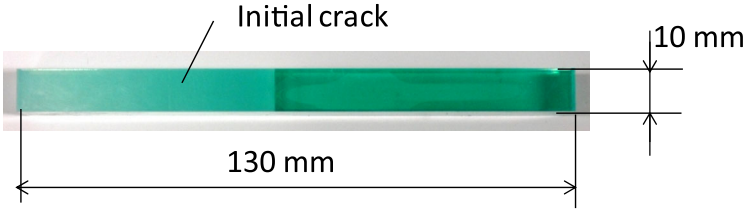

Figure 4. Specimen and its dimensions. The total thickness of the specimen is 20 mm. This figure is published in color on http://www.ingentaconnect.com/content/vsp/acm

used as starter cracks. Then, the glued plate was machined to specified dimensions. The dimensions of the specimen are given in Fig. 4.

Some natural crack was introduced by mode I loading condition before the tests. The cross-head speed was set at 0.25 mm/min. The crack propagation was recorded by a digital video camera. The crack shape $c(y)$ was measured through the video camera images after the test.

2.3. Experimental Results

A relationship between the applied load and the displacement of the cross-head and ongoing change of a crack front shape recorded using a video camera at several load points are shown in Figs 5 and 6, respectively. The numbers in the figures show the corresponding instant of the test. The crack growth initiated from the edge of the originally straight crack as shown in the picture 1 of Fig. 6. With the increase of the applied displacement, the crack spread to the middle of the specimen. Then, the applied load gradually decreased with the decrease of the stiffness of the specimen due to the whole crack propagation from point 2 (Fig. 5). The crack propagation was quite stable until the end. The continuous load–displacement curve suggests that the crack grew stably. The critical condition of the crack propagation is attained at all

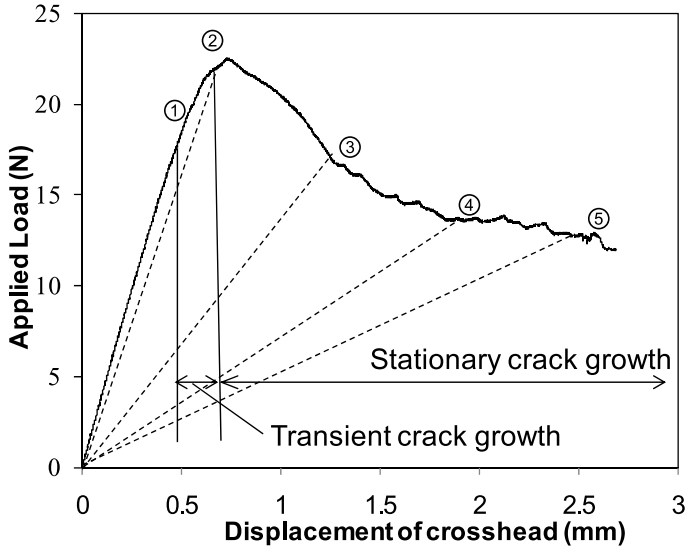

Figure 5. Load–displacement curve and profiles of crack front of an acrylic resin specimen.

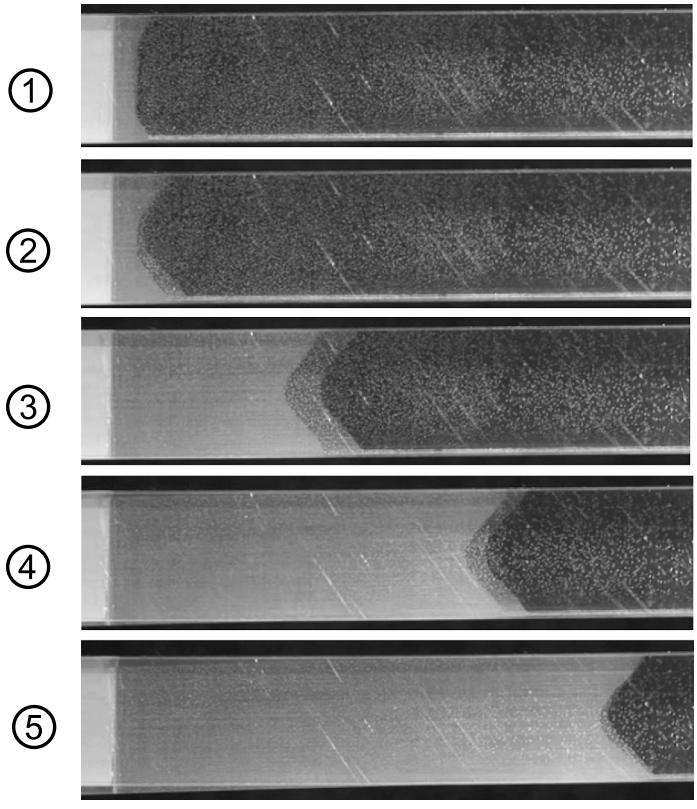

Figure 6. Profiles of crack front of an acrylic resin specimen.

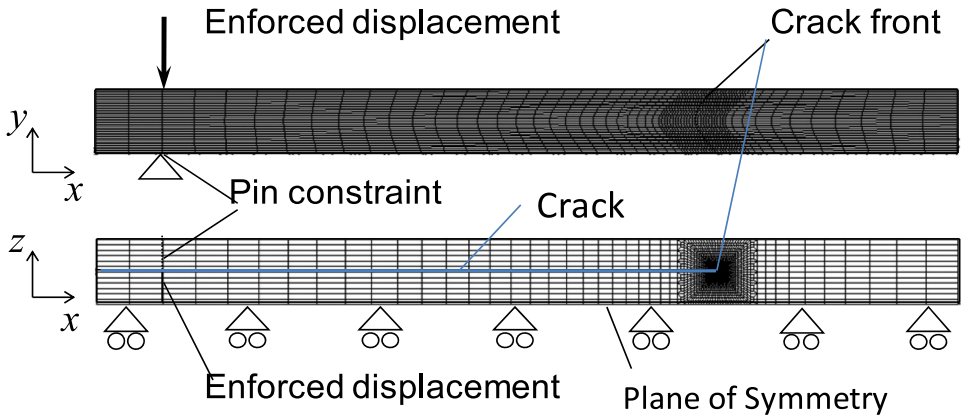

Figure 7. Finite element mesh and boundary conditions. This figure is published in color on http://www.ingentaconnect.com/content/vsp/acm

the points along the curved crack front. The crack, being almost symmetric with the centerline of the specimen, took almost the same shape during crack propagation as shown in pictures 1–5 in Fig. 6. The sizes of the two cracks tended to be equal, though some difference existed because of the difference of the toughness of the interfaces, probably due to non-uniform adhesive thickness and quality. However, the difference of the crack length is not essential for the evaluation of the toughness as long as the difference is small compared to the crack length.

2.4. Finite Element Analysis

Finite element analyses (ABAQUS 6.61) were conducted to evaluate the energy release rate distribution along the measured crack front $c(y)$. Continuous curve $c(y)$ was interpolated by a spline curve from the finite number of the measured distances along the crack front. A finite element model is shown in Fig. 7. Utilizing the symmetry condition, only a half of the specimen was analyzed with eight-noded brick element C3D8. A finer mesh was used in the region near the crack front to obtain a more accurate result. Material properties used in the analyses were determined by referring to the catalog values. Young's modulus E and Poisson's ratio ν of the acrylic resin are 2.9 GPa and 0.39, respectively. The energy release rate was calculated with the virtual crack closure technique.

3. Results and Discussion

The energy release rate distribution for the case of straight crack ($c = 50$ mm, $\delta = 2$ mm) is plotted against normalized position y/h in Fig. 8. The mode I component was negligible as expected. The mode II component relates to the bending stress, while the mode III component relates to the shear stress as well as Poisson ratio effect near both sides, where one cracked portion is in tension and the other in compression. The energy release rate is large near the side of the specimen where the crack started growing in the test, as shown in the photographs 1 and 2 of Fig. 6.

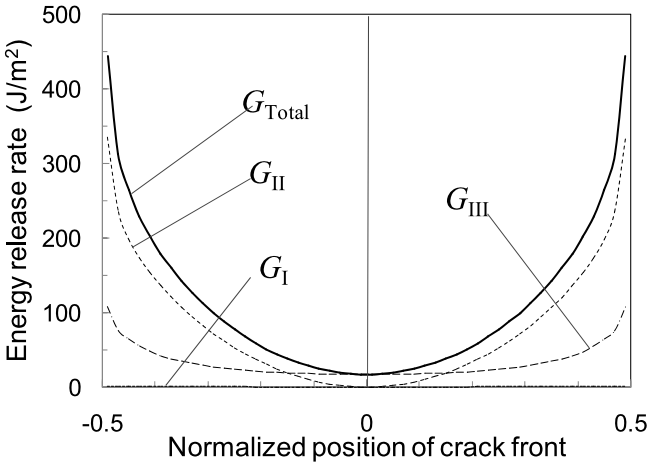

Figure 8. Energy release rate distribution along a straight crack front at the applied displacement is 2 mm.

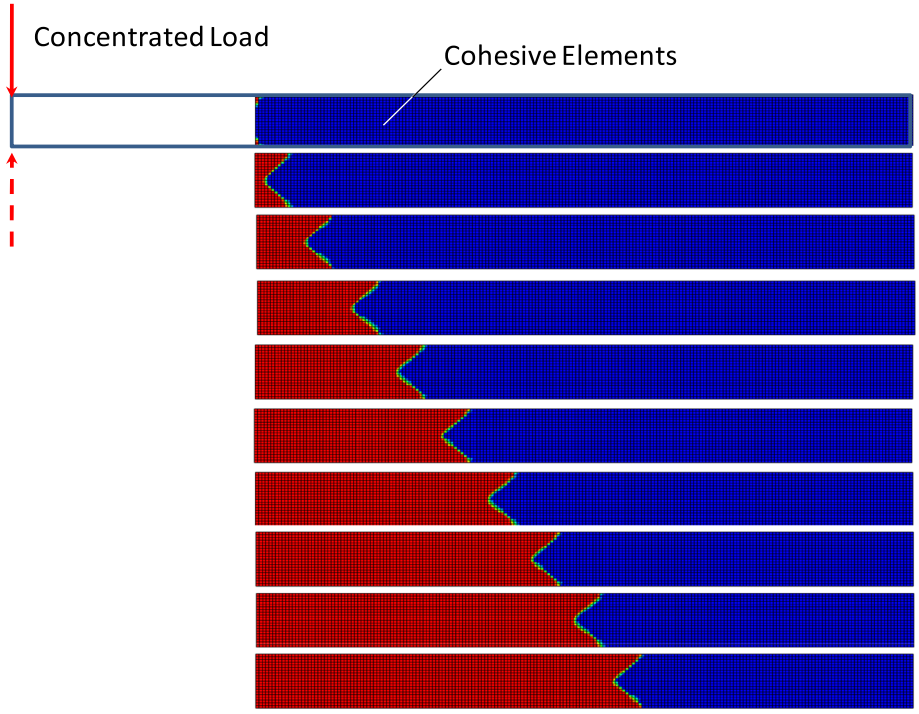

Figure 9. Crack propagation history numerically obtained by using a cohesive element when $G_{IIc} = G_{IIIc}$. Height of specimen = 10 mm and initial crack length = 50 mm. This figure is published in color on http://www.ingentaconnect.com/content/vsp/acm

The result of a crack propagation simulation using cohesive element assuming $G_{IIc} = G_{IIIc}$ is shown in Fig. 9. The result was successfully obtained and the crack

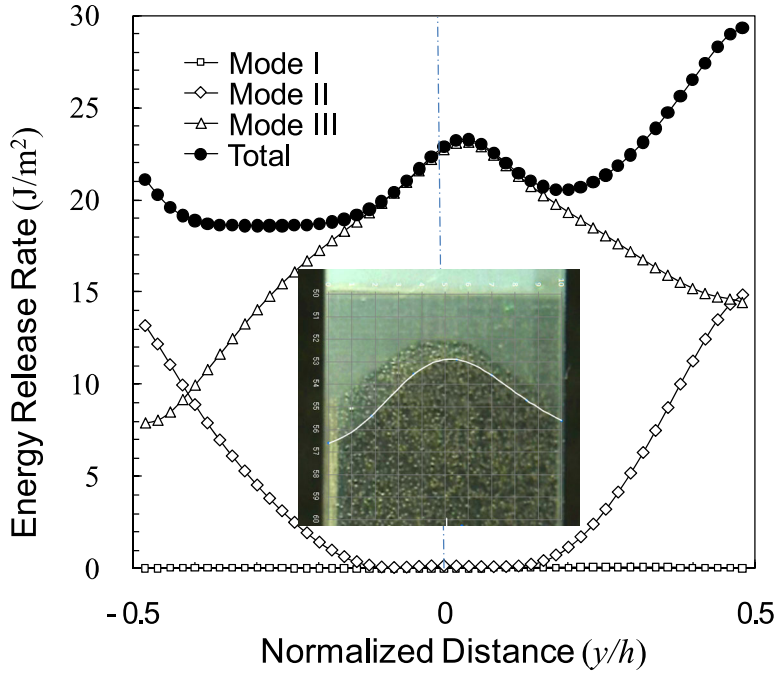

Figure 10. Total and each energy release rate distribution along the crack front when the applied displacement is 0.65 mm. This figure is published in color on http://www.ingentaconnect.com/content/vsp/acm

growth history was quite similar to the experiment (Fig. 6). This shows that the energy release rate can be estimated once the crack shape is observed.

The energy release rate distributions at the stages 2 and 4 of Fig. 6 are shown with the crack shapes in Figs 10 and 11. The mode II component, being zero at the center of the crack front, increases with the distance from the center line of the beam. On the other hand, the mode III component, being maximum at the center point, decreases basically with the distance. The tendencies are similar for all the cases. The mode II component is almost zero in the quite wide area near the center portion and almost pure mode III failure was realized near the centerline. The fracture toughness tended to be large near the center line of the specimen in spite of the fact that a mode II component does not exist. The gradual decrease of the mode III fracture toughness with the distance from the center line might be caused by an inaccurate measurement of the crack-front curves due to the unclear video images. We will mention the sensitiveness of the measured crack profile later. The energy release rate tended to be large near the edge area, probably because of the edge effect.

The relation of G_{II} and G_{III} components are plotted just at the crack instability in Fig. 12. The data just at the edge were omitted from the figure. The horizontal axis is the mode II component and the vertical axis shows the mode III component.

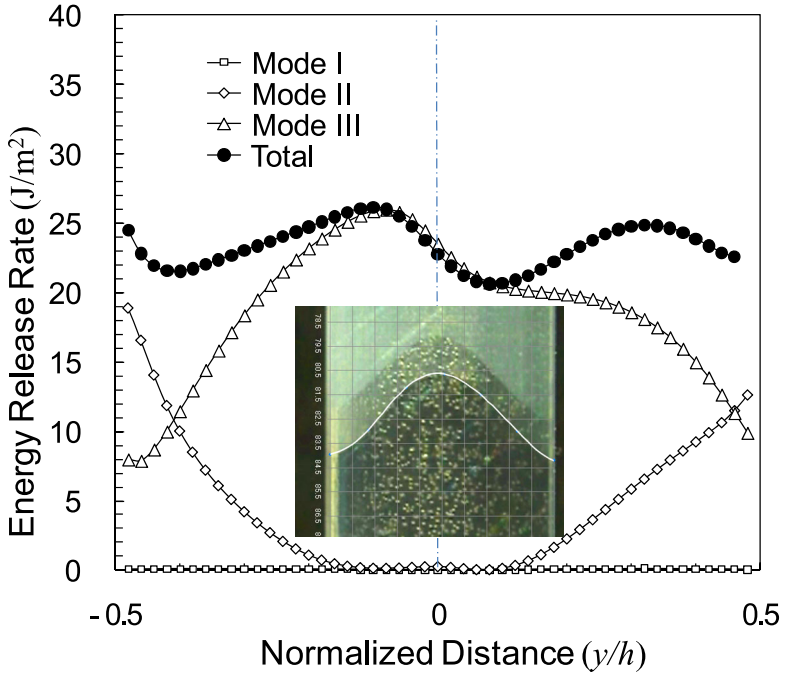

Figure 11. Total and each energy release rate distribution along the crack front when the applied displacement is 1.71 mm. This figure is published in color on http://www.ingentaconnect.com/content/vsp/acm

Mean values of the results are indicated by a broken line. The fracture criterion for mixed mode condition (mode II and III) may be obtained from the present test method.

The values of the critical total energy release rate and each energy release rate component are dependent on the measured crack size and shape. If the measured total length of the crack is incorrect and the shape is correct, the error of the calculated energy release rate is caused by the difference of the magnitude of the bending moment at the crack front, which is proportional to the crack length. So, the error of the critical energy release rate due to the average length difference is not significant, because the order of relative error of the crack length is usually small. The effect of the measured shape on the energy release rate was studied by comparing the energy release rate distributions for three crack profiles, as shown in Fig. 13. The crack profiles were obtained by changing the data of the point No. 3 of the original crack data shown in Fig. 11 by ± 0.5 mm and interpolating the profiles by spline functions. The interpolated shapes by the spline function have a little wavy form. The obtained energy release rate distributions are plotted in Fig. 14. The strong dependency on the measured crack profile is observed in the figure. Fortunately, the effect of the profile difference is not clear on the other side of the crack front. The energy release rate is overestimated at the portion where the crack is determined longer than the

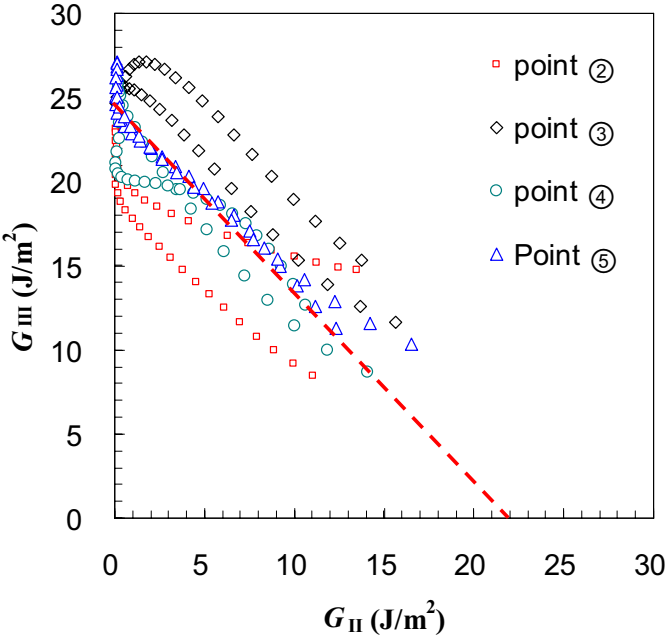

Figure 12. Mixed mode ratio of critical energy release rate. This figure is published in color on http://www.ingentaconnect.com/content/vsp/acm

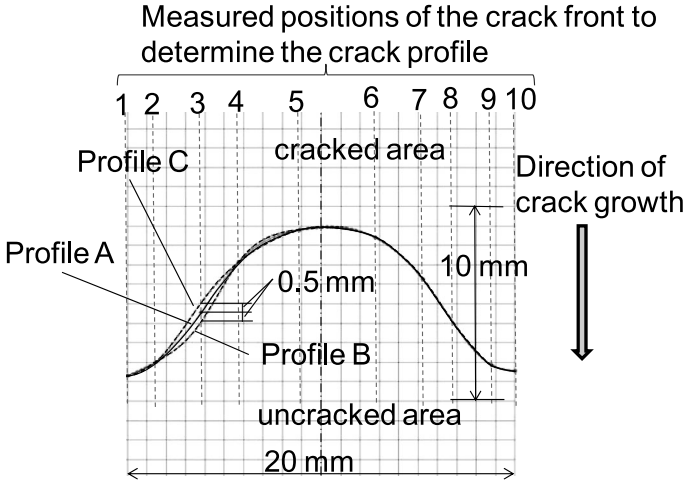

Figure 13. The different crack shapes to study the effect of the sensitivity of the measured profile of the crack. The profile A is the crack shape when the applied displacement is 1.71 mm.

real length; of course, it is, therefore, underestimated where the crack is determined shorter. The difference of the energy release rate distribution is several times larger than the crack profile difference. So, the measurement of the crack profile must be carefully done to avoid the inaccuracy of the results.

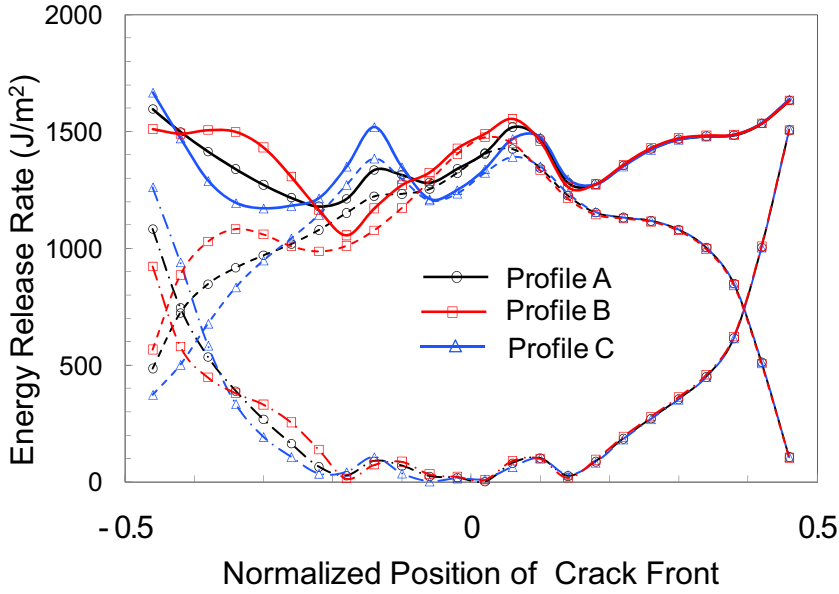

Figure 14. Effect of the measured crack profile on the distribution of the total energy release rate and the mode II and III components. This figure is published in color on http://www.ingentaconnect.com/content/vsp/acm

4. Conclusions

A double-notched split cantilever beam test was proposed to evaluate mixed mode II and III fracture toughnesses. Experimental and finite element studies were demonstrated to show the applicability of the present method. We found that the crack grew stably with the increase of the applied displacement and formed a curved crack front along which the critical condition was achieved. The finite element analyses were suitable to evaluate the critical energy release rate along the crack front. This could provide a powerful test method for mixed mode II and III fracture toughnesses as long as the crack profiles can be accurately defined.

Acknowledgements

Part of the present research was supported by Grant-in-Aid for Scientific Research (C) (17560080). We also acknowledge the support of Japan Aerospace Exploration Agency as co-research project.

References

1. J. M. Whitney, Stress analysis of the double cantilever beam specimen, *Compos. Sci. Technol*. **23**, 201–219 (1985).

2. J. R. Wilkins, R. A. Eisenmann, R. A. Camin, W. S. Margolis and R. A. Benson, Characterizing delamination growth in graphite–epoxy, damage in composite materials, *ASTM STP* **775**, 168 (1980).
3. W. D. Bascom, R. J. Bitner, R. J. Moulton and A. R. Siebert, The interlaminar fracture of organic–matrix woven reinforced composites, *Composites* **11**, 9–18 (1980).
4. S. S. Wang, H. Suemasu and N. Zahlan, Interlaminar fracture of random short-fiber SMC composite, *J. Compos. Mater*. **18**, 574–594 (1984).
5. H. Suemasu, H. Hososda and K. Nara, An experimental study of interlaminar toughness of satin woven fabric composite, *J. Japan Soc. Compos. Mater*. **13**, 225–232 (1987).
6. L. A. Carlsson, J. W. Gillespie and R. B. Pipes, On the analysis and design of end notched flexure (ENF) specimen for measuring mode II fracture toughness, *Compos. Sci. Technol.* **20**, 594–604 (1986).
7. G. Becht and J. W. Gillespie, Design and analysis of crack rail shear specimen for mode III interlaminar fracture, *Compos. Sci. Technol*. **31**, 143–157 (1988).
8. S. M. Lee, An edge crack torsion method for mode III delamination fracture toughness, *J. Compos. Technol. Res. JCTRER* **15**, 193–201 (1993).
9. W. C. Liao and C. T. Sun, The determination of mode III fracture toughness in thick composite laminates, *Compos. Sci. Technol*. **56**, 489–499 (1996).
10. H. Suemasu, On an experimental method to measure mode III interlaminar fracture toughness of composite laminates, *Compos. Sci. Technol*. **59**, 1015–1021 (1999).
11. H. Yoshihara, Examination of 4-ENF test for measuring the mode III R-curve of wood, *Engng Fract. Mech*. **73**, 42–63 (2006).
12. A. Szekrenyes, Delamination fracture analysis in the G_{II}–G_{III} plane using prestressed transparent composite beams, *Intl J. Solids Struct*. **44**, 3359–3378 (2007).
13. A. B. de Morais and A. B. Pereira, Mixed mode II + III interlaminar fracture of carbon/epoxy laminates, *Compos. Sci. Technol*. **68**, 2022–2027 (2008).
14. S. L. Donaldson, Mode III interlaminar fracture characterization of composite materials, *Compos. Sci. Technol*. **32**, 225–249 (1988).